ORIGINAL ARTICLE

Dual cardiac–respiratory gated PET: implementation and results from a feasibility study

Axel Martinez-Möller · Darko Zikic · René M. Botnar ·
Ralph A. Bundschuh · William Howe ·
Sibylle I. Ziegler · Nassir Navab · Markus Schwaiger ·
Stephan G. Nekolla

Abstract

Purpose Spatial resolution in myocardial imaging is impaired by both cardiac and respiratory motion owing to motional blurring. We investigated the feasibility of a dual cardiac–respiratory gated positron emission tomography (PET) acquisition using a clinical PET/computer tomography (CT) scanner. We describe its implementation and present results on the respiratory motion observed.

Methods The correlation between diaphragmatic excursion measured by real-time magnetic resonance imaging (MRI) and the expansion of the chest measured with an elastic belt was studied in six subjects. PET list mode acquisitions were then performed in 12 patients, six of them injected with ^{13}N-ammonia and six with ^{18}F-FDG. In parallel, the ECG and respiratory signals of the patients were recorded and the list mode file correspondingly sorted using a dual gated approach. Respiratory motion of the heart was quantified by measuring the displacement between the inspiratory and expiratory images in the diastolic phase by means of intensity-based non-rigid image registration.

Results The correlation between diaphragmatic excursion and expansion of the chest was excellent ($R^2=0.91$), validating the ability of the elastic belt to provide an adequate respiratory trigger. Respiratory signals corresponding to the chest expansion showed a large inter-patient variability, requiring adapted algorithms in order to define suitable respiratory gates. Dual gated PET series were successfully acquired for both groups of patients, showing better resolved myocardial walls. The average respiratory motion of the heart measured by PET was 4.8 mm, with its largest component in the craniocaudal direction. Moreover, a deformation of the heart with respiration was observed, with the inferior wall moving significantly more than the anterior.

Conclusion Dual gated cardiac PET studies were performed successfully and showed better resolved myocardial walls as compared with ungated acquisitions. The respiratory motion of the heart presented a significant elastic component and was of the same magnitude as the spatial resolution of current PET cameras.

Keywords PET · Cardiology · Respiratory gating · Registration

A. Martinez-Möller · R. M. Botnar · R. A. Bundschuh ·
S. I. Ziegler · M. Schwaiger · S. G. Nekolla
Nuklearmedizinische Klinik der Technischen Universität
München,
Munich, Germany

A. Martinez-Möller (✉) · D. Zikic · N. Navab
CAMP-AR, Computer Science Department, TU München,
Munich, Germany
e-mail: a.martinez-moller@lrz.tu-muenchen.de

W. Howe
Molecular Imaging, Siemens Medical Solutions,
Knoxville, TN, USA

Introduction

Positron emission tomography/computed tomography (PET/CT) has the potential to be a valuable tool in non-invasive cardiac imaging [1]: the PET quantitative measurements of myocardial blood flow, coronary flow reserve and tissue viability [2, 3] are complemented by the anatomical information and morphology of the stenoses as observed with CT [4]. With a spatial resolution below 5 mm in commercial PET scanners [5], further possibilities for cardiovascular imaging with PET are currently under research, such as the discrimination between subendocardial and subepicardial blood flow [6], the characterization

of plaque vulnerability by co-registration with computed tomography angiography (CTA) [7] or imaging of cardiac reporter gene expression [8].

The effective resolution in cardiac PET, however, is significantly worse than the nominal spatial resolution obtained in phantom measurements as a result of combined cardiac–respiratory motion [9]. For instance, coronary arteries have been shown to move 8–23 mm during the cardiac cycle [10], whereas values reported for the respiratory motion of the heart and coronaries during free breathing range between 4.9 and 9.0 mm [11–13]. Therefore, cardiac PET can only exploit the spatial resolution available in state-of-the-art scanners with techniques to account for both respiratory and cardiac motion. A pioneering study indicated the feasibility of such an approach using dual cardiac–respiratory gating in phantoms [14], but technical limitations were reported (real-time definition of the gates, partial loss of data, maximum of 16 gates in total) and the method was not implemented in clinical practice. In mouse imaging, recent implementation of combined cardiac–respiratory gating in the preclinical microPET II scanner overcame these limitations [15]. This methodological achievement, however, proved unnecessary in this animal model as mice remain in an end-expiratory state for more than 75% of the time. In contrast, the end-expiratory state represents only 25–50% of the human natural breathing cycle and respiratory motion may play a more significant role. Recently, respiratory gating was also proposed for clinical cardiac PET [16], but the combination with ECG gating was not investigated.

The purpose of this study was to show the feasibility of a simultaneous cardiac–respiratory gated PET acquisition using a clinical PET/CT.

Materials and methods

MR acquisition for validation of the respiratory triggering

The correlation between diaphragmatic excursion measured by real time MR and the expansion of the chest measured with an elastic belt was studied in six subjects. The subjects were examined using a clinical 1.5-Tesla Philips ACS-NT MR (Philips Medical Systems, Best, The Netherlands) equipped with a five-element cardiac coil and an advanced cardiac software package (R11). Real-time MR of the lung–liver interface was performed in a coronal plane using a non-electrocardiogram (ECG) triggered single-shot Cartesian steady state free precession (SSFP) sequence. Imaging parameters included: TR/TE 2.5 ms/1.25 ms, flip angle 50°, spatial resolution $3.2 \times 3.2 \times 8.0$ mm, temporal resolution 182 ms, dynamics 100, and SENSE factor 2 (SENSitivity Encoding). Simulta-

neous with the MR real-time measurement, the signal corresponding to the thorax expansion was measured with a small pressure pad placed within a stretchable belt on the upper abdomen. A respiratory signal was derived from the air flow variations and recorded into a log file in the MR acquisition computer together with timing information necessary to synchronize the signal with the corresponding MR acquisition. This system is standard equipment with the used MR scanner.

The diaphragmatic excursion due to respiration has been shown to correlate with the respiratory motion of the heart with a patient-dependent linear factor [13, 17]. Thus, if the measured respiratory signal provides an adequate trigger to monitor the diaphragm excursion, the trigger will equally serve for the respiratory motion of the heart, as used for cardiovascular MR using diaphragmatic navigators.

The displacement of the diaphragm was measured from the sequence of images by quantifying the craniocaudal motion of the liver–lung interface within a two-dimensional region of interest (ROI), then compared with the respiratory signal obtained from the elastic belt by means of the linear Pearson correlation coefficient.

Patient population

Twelve patients belonging to two different groups were included in the study: six of the patients (age 61 ± 13 years) were referred for diagnosis of coronary artery disease and underwent a ^{13}N-ammonia (NH$_3$) perfusion examination, consisting of an acquisition at rest and one during adenosine-induced stress. The remaining six patients (age 67 ± 6 years) were originally referred for an ^{18}F-fluorodeoxyglucose (FDG) oncology examination and were included in the study owing to their intense cardiac uptake. Using these two groups of patients, the gating approach could be tested with short-lived perfusion radiotracers as well as with long-lived metabolic radiotracers and thus represents tracers typically used in cardiac PET imaging. Patients provided informed consent.

PET/CT acquisition

All 12 patients were scanned using a Biograph Sensation 16 PET/CT (Siemens Medical Solutions, Erlangen, Germany) for 10 min and the data were stored in listmode format, that is, each detected coincidence event was recorded with millisecond temporal resolution into a file as a 32-bit word representing the couple of crystals detecting the coincidence. The average injected dose was 256 ± 35 MBq of ^{13}N-ammonia for the rest acquisition and 295 ± 61 MBq for the stress acquisition in the first patient group, and 400 ± 62 MBq of ^{18}F-FDG in the second patient group. The PET acquisition was started synchronized with the tracer
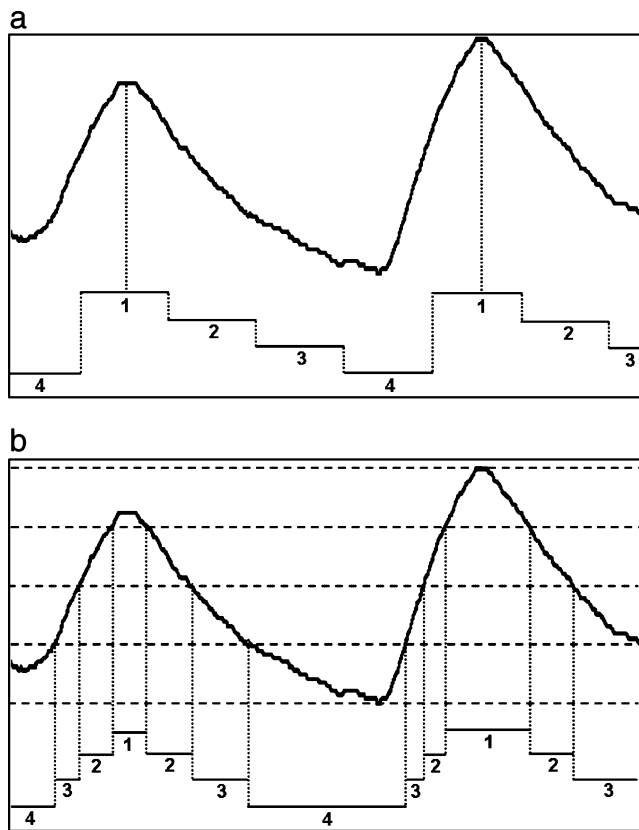
Fig. 1 Definition of the respiratory gates using two different algorithms: **a** based on equitemporal division of the respiratory cycles; **b** based on the intensity division of the signal range

injection for the ammonia patients and 60 min after injection for the FDG patients.

In parallel to the listmode acquisition, the ECG provided with the PET/CT scanner recorded the exact timing of the R waves in a binary log file on the PET acquisition computer. The respiratory state of the patient was measured with the Anzai AZ-733V system (Anzai Medical Co., Tokyo, Japan), based on the same principle as the sensor used in the MR experiment, that is, to measure the expansion of the chest by means of a pressure sensor. The system, initially conceived for respiratory gated radiotherapy, is constituted by a pressure transducer which is positioned inside a pocket on an elastic belt, itself placed on the upper abdomen of the patient. The pressure transducer is connected to a device comprising all acquisition electronics (Anzai Wave Deck) which samples the respiratory signal every 25 ms and delivers it to a separate laptop which stores it into a formatted text file.

In order to achieve accurate temporal synchronization between the listmode and ECG acquired by the PET terminal and the respiratory signal acquired by the separate laptop, the PET terminal was programmed to send an output signal on the parallel port when the listmode acquisition started, and this signal was transferred via a customized parallel-serial converter to the Anzai Wave Deck and stored together with the respiratory signal.

For attenuation correction, a low-dose CT (120 keV, 20 mAs) was performed during shallow breathing. In order to reduce attenuation artefacts due to the misregistration of the PET and CT datasets [18], the alignment of the heart between the PET and CT volumes was visually controlled immediately after the PET acquisition, and in those patients presenting a misalignment, an additional ultra-low-dose CT (80 keV, 13 mAs) was acquired.

All data required for the dual gated reconstruction (listmode file, ECG, respiratory signal and CT-based attenuation map) were transferred through the network to another computer for offline processing, so that the PET/CT scanner could be further used. Therefore, the dual gated acquisition had no effect on the usual clinical workflow other than the addition of the elastic belt to measure the respiratory signal. Finally, the PET images were reconstructed using the attenuation-weighted ordered subsets expectation maximization (AW-OSEM) algorithm with four iterations and eight subsets and an in-plane zoom of 2.2 to a matrix of $128 \times 128 \times 47$ voxels, each voxel with a size of $2.34 \times 2.34 \times 3.37$ mm^3.

Definition of the gates

The cardiac and respiratory gates were defined retrospectively using the Interactive Data Language (IDL, RSI Inc, Boulder, CO). The definition of the cardiac gates was achieved by dividing the interval between two consecu-

Fig. 2 Different combinations to sort a dual gating matrix with eight cardiac and eight respiratory gates. **a** Cardiac gated series. **b** Respiratory gated series. **c** Respiratory gated series after exclusion of the systolic phase
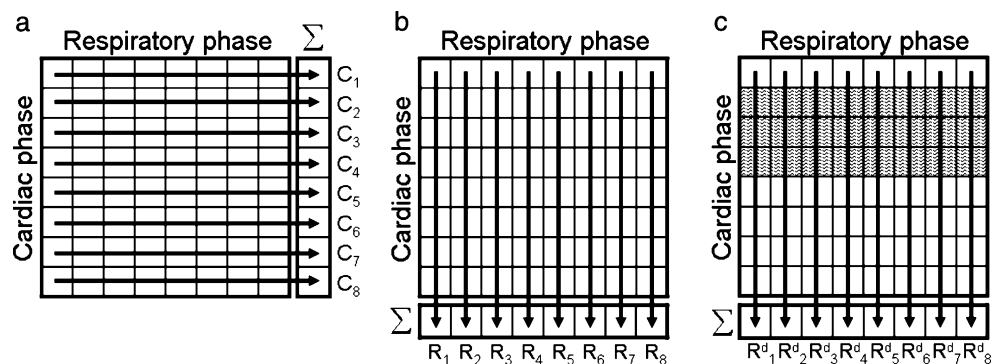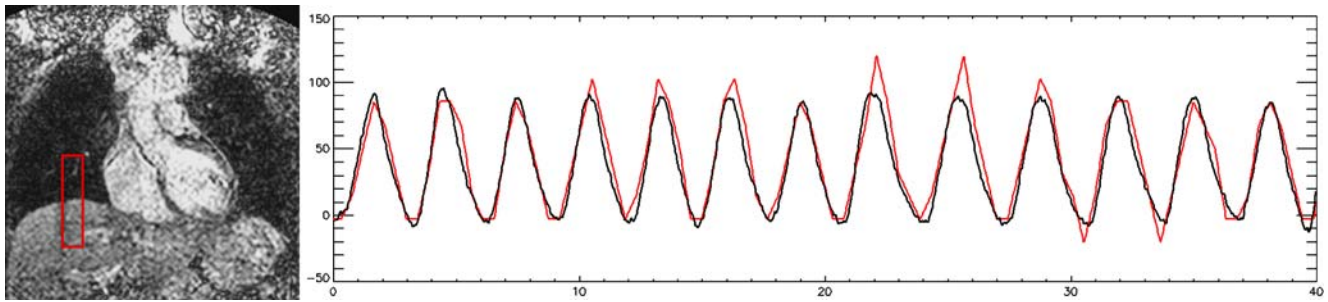
Fig. 3 MR coronal image showing the definition of the ROI at the liver–lung interface and comparison of both signals: red signal obtained from the diaphragmatic excursion in the ROI, black signal obtained from the stretchable belt. The amplitude ranges of both signals were adjusted to similar values in order to facilitate visual comparison

tive R waves into n frames of the same duration, n being the desired number of gates. The computation of the respiratory gates out of the respiratory signal required some additional signal processing. The noise in the acquired signal was reduced by means of a bandpass filter (0.05–0.6 Hz) and a gating algorithm comparable to the one for cardiac gating was applied, where the interval between two consecutive inspiration peaks was divided into m frames of the same duration, m being the number of respiratory gates (Fig. 1a). As compared with an intensity-based gating algorithm (Fig. 1b), which was also tested but discarded for this study, this gating approach presents two significant advantages: it delivers equitemporal gates, which therefore have similar count statistics, and it is robust to changes in the baseline of the signal, as discussed later.

Thus, a matrix of n times m gates was obtained, with one dimension corresponding to the cardiac beating motion and the other to the respiratory motion (Fig. 2). Finally, these gates could be combined flexibly during the sorting process. For example, if eight cardiac gates were defined, the user could define a diastolic inspiratory image consisting of the cardiac gates 1 and 5–8 combined with gate 1 from the respiratory dimension (Fig. 2c).

Although a substantial part of the hardware and software we used was provided by Siemens, the technical implementation of respiratory gating and its combination with cardiac gating was developed on-site and does not correspond to a product from the manufacturer.

Motion analysis

In order to quantify exclusively the respiratory motion of the heart, the systolic phase of the heart was discarded as indicated in Fig. 2c. The images corresponding to maximum inspiration and maximum expiration were registered using the deformable registration algorithm described in the following paragraph and the resulting motion was evaluated for each of the myocardial walls. The analysis was performed using four and eight respiratory gates.

The used deformable registration algorithm is an intensity-based and fully automatic method yielding a dense displacement field. We employed a variational method for deformable registration utilizing the sum of squared differences as a dissimilarity measure and a diffusion regularization term to enforce smooth results [19]. The resulting non-linear elliptic partial differential equation (PDE) was solved by a modified fixed-point iteration where a linear elliptic PDE arose in every iteration. The linear PDE was solved numerically by applying an efficient multigrid algorithm [20]. In order to improve the computation time and account for large displacements, we employed a multi-resolution pyramid [21]. The pyramid was computed by reducing the resolution by a factor of 2 along each dimension from level to level by applying a discrete approximation to the Gaussian filter. On every level of the pyramid, the deformable registration was performed using the result of the next coarser level as an initial guess. The registration algorithm was implemented in C++ and the runtime for a pair of PET volumes of size $128 \times 128 \times 47$ was 6–7 s on a Pentium M 1.8-GHz computer.

Results

Validity of the respiratory trigger

The correlation between the image-derived excursion of the diaphragm extracted from the real-time MRI and the signal from the stretchable belt was excellent (mean R^2 of 0.91, range 0.88–0.94), indicating the ability of the belt to provide a suitable respiratory trigger signal (Fig. 3).

Variability of the respiratory signals

The respiratory patterns from the PET patients showed a very large interindividual variability (Fig. 4) for both the ammonia and the FDG patients. This variability had not been observed during previous testing experiences with
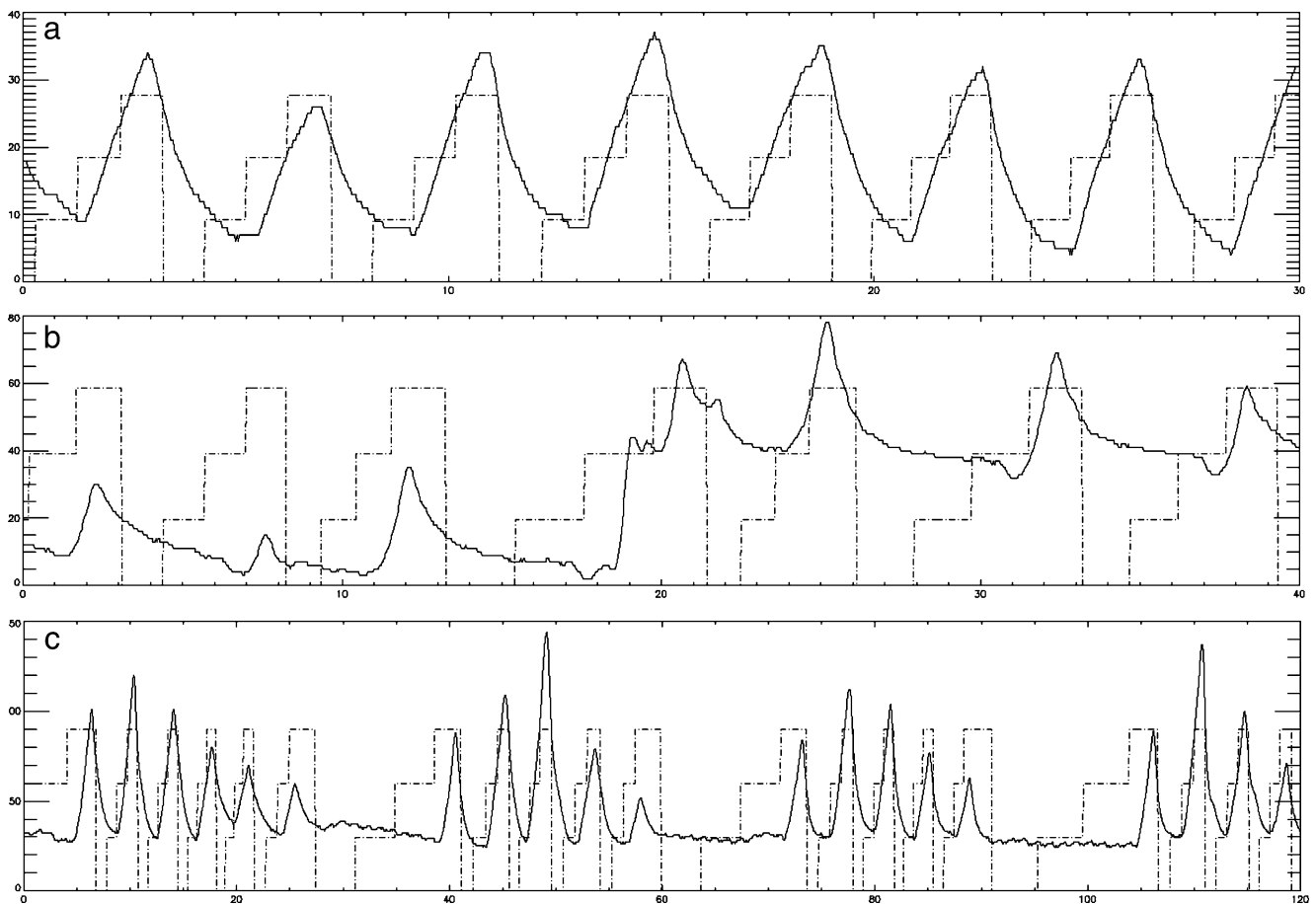
Fig. 4 Fragments of three respiratory signals acquired from patients (*solid curves*) and the corresponding respiratory gates (m=4) as defined by the applied algorithm. Half of the patients had a respiratory pattern fairly similar to **a**, but the other half had rather unusual patterns, two of which are presented in **b** and **c**. Signal **b** also shows a sudden change of the baseline, probably introduced by a slight repositioning of the patient

the respiratory sensor in young healthy volunteers, indicating that several patients could have respiratory abnormalities probably related to their health condition. Moreover, small irregularities in the respiratory signals were common, including very deep breathing, occasional speaking or coughing, and sudden or progressive changes in the baseline. The employed gating algorithm was robust to the different patterns and irregularities observed in the signals; in particular, changes of the baseline during the examination were handled efficiently by the temporal division of the breathing cycles, whereas the approach using intensity division failed to account for these changes.

Respiratory motion of the heart

The respiratory motion of the heart is observable in Fig. 5 on both the PET images and the activity profiles. The activity profiles show that the myocardial wall in the static image appears thicker and with reduced maximum activity as a result of the motional blurring, indicating the potential improvement of spatial resolution that can be achieved by means of respiratory and dual gating.

Results of the non-rigid registration are presented in Fig. 6, showing that the heart followed mainly a cranio-caudal displacement with respiration. The average respiratory motion of each myocardial wall for all examinations is shown in Table 1. The average motion of the entire heart for each group of patients was 4.9±1.3 mm for the ammonia rest acquisitions, 5.0±2.7 mm for the ammonia stress acquisitions and 4.6±1.3 mm for the FDG acquisitions. The motion for all 18 examinations averaged 4.8± 1.8 mm. Changing the number of respiratory gates used from four to eight produced a significant increase in the motion extent (3.92 vs 4.82 mm average motion, $p<0.001$) as a consequence of the better temporal resolution of the gates.

Combined with the craniocaudal displacement, we observed a deformation of the heart during respiration, with the inferior wall presenting a significantly larger motion than the anterior wall (5.84 vs 4.16 mm average motion, $p<0.001$).
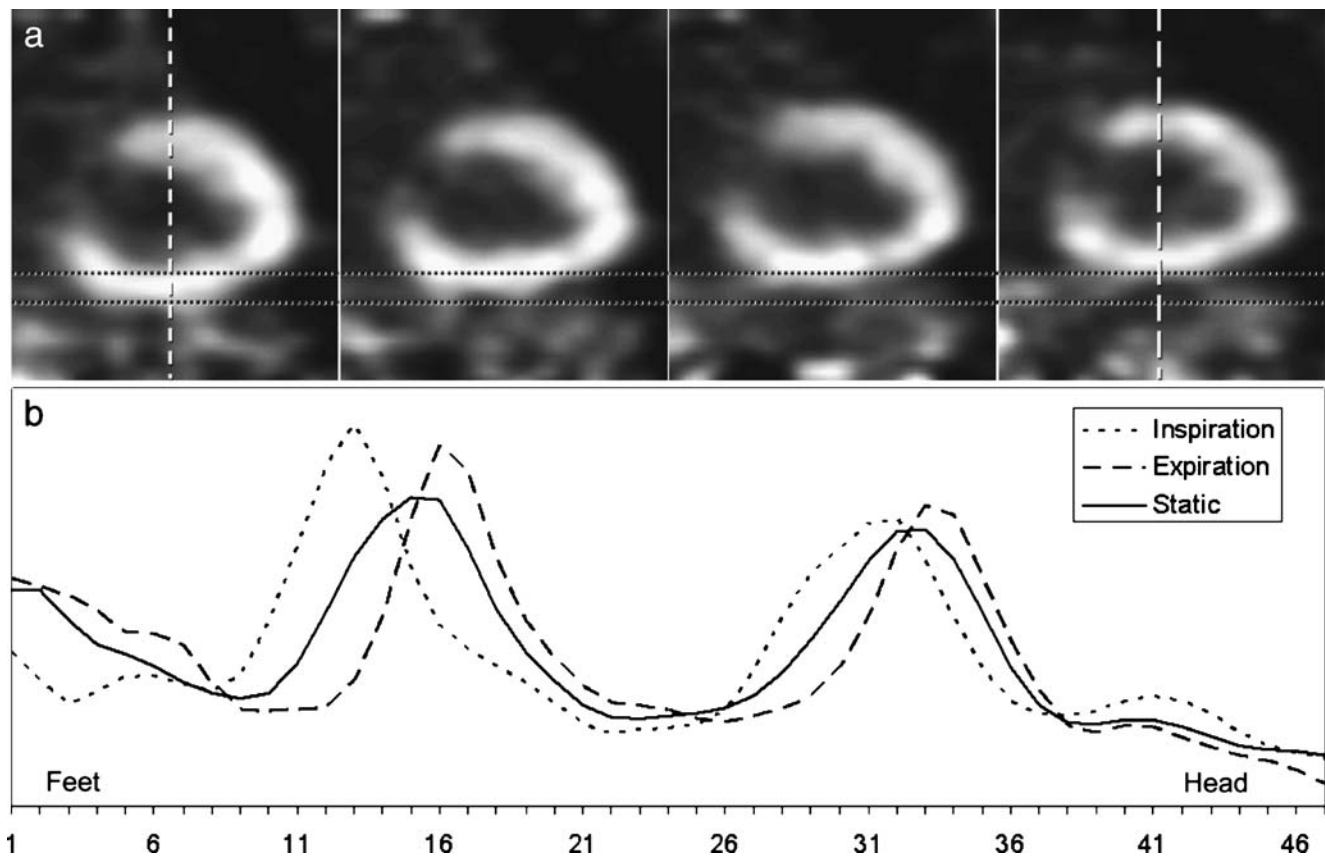
Fig. 5 Data from an examination with 10-mm feet–head respiratory motion at the inferior segment of the heart. **a** Coronal view of the respiratory gated images in the diastolic phase. **b** Craniocaudal activity profile through the left ventricle showing the displacement of the myocardial walls with respiration

Discussion

This study showed the feasibility of a dual cardiac–respiratory gated PET acquisition using a clinical PET/CT scanner. Respiratory motion of the heart averaged 4.8 mm, which is comparable to the spatial resolution of current clinical PET scanners. The motion showed significant local differences: the inferior wall of the heart moved 5.8 mm on average, 40% more than the anterior wall, indicating that the heart is not only moving craniocaudally with respiration, but also deforming. This deformation could be an

indicator of a potential variation in left ventricular preload with respiration.

The observed average respiratory motion of the heart (4.8 mm) is a rather low value as compared with other data in the literature. This is a consequence of important differences in the methodology: one essential factor is how breathing is performed. Some MR studies have reported respiratory motion measured comparing breath-holding at inspiration and expiration [22], motion which is known to be higher than that observed during free breathing, as in the case of our study. A second difference

Fig. 6 Displacement field resulting from the non-rigid image registration between inspiratory and expiratory phases. The displacement vectors are plotted on top of the image in the axial, coronal and sagittal views
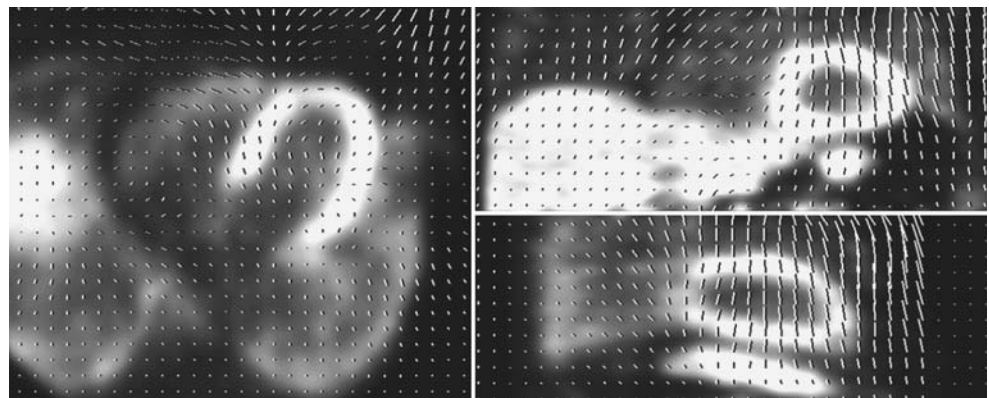
Table 1 Average respiratory motion (mean ± standard deviation) in millimetres for the 18 PET examinations

			Myocardial segment				
			Anterior	Septal	Inferior	Lateral	Apex
4 gates		CC motion	3.2±1.6	3.8±1.6	4.4±2.0	3.7±2.1	3.1±1.5
		3D motion	3.4±1.6	4.1±1.5	4.7±2.0	4.0±2.1	3.4±1.6
8 gates		CC motion	4.0±1.5	4.5±1.8	5.5±2.2	4.6±2.1	3.8±1.8
		3D motion	4.2±1.5	4.9±1.8	5.8±2.2	4.9±2.2	4.3±1.7

CC craniocaudal

is the population examined. Reports from MR studies are frequently based on young healthy volunteers, whereas the population included in our study consisted of CAD and cancer patients with an average age of 64 years; clear differences between motion in volunteers and patients can be seen in [22], where young volunteers showed an average craniocaudal motion of 16 mm and the patients (age 56± 9 years) a motion of 8 mm. Finally, in our study we report on the average motion for the entire heart, but we also observe that this motion is not homogeneous and, in particular, the inferior wall shows a higher motion (5.8 mm); for comparison, a recent study including eight young healthy subjects showed an average motion at the infero-apical extreme of the heart of 6.7 mm [12].

A study which compares well in the patient population (65±11 years) and also uses free-breathing acquisition is that by Shechter et al. [11]; during free-breathing coronary angiograms, the heart was reported to have an average craniocaudal motion of 4.9±1.9 mm, in agreement with our measurements.

Dual gating suffers from the problem of low statistics: the gain achieved by the reduction of motion blurring involves a significant loss of count statistics. If the same histogramming approach as for "single" gating is used, image quality is significantly reduced: for instance, when using eight cardiac gates and eight respiratory gates, the total counts are divided by 64. The reduction of count statistics derived from dual gating can potentially be overcome by spatial registration. That is, all respiratory gates can be registered to the expiratory gate and summed into one respiratory-free image with high counts. Although rigid registration has been

proposed for this purpose [23], our measurements indicate that the motion is not uniform across the left ventricle, a finding which is supported by previous studies [22, 24, 25]. Thus, a non-rigid correction will provide greater accuracy.

As an alternative to image registration, the selection of only those parts of the cardiac and respiratory cycles where minimal motion is present provides a suitable approach. Respiratory patterns suggest that end-expiration may be the most suitable part of the respiratory cycle as it has the longest period without motion. Thus, approximately 25–50% of the data could be considered to have nearly no respiratory motion. The same applies for ventricular diastole, which represents more than 60% of the cardiac cycle depending on the degree of ventricular dysfunction. By combining both, 15–30% of the total acquired data could be considered to have virtually no motion, cardiac or respiratory, so that a motion-free image of the heart could be obtained without the use of any registration technique (Fig. 7).

A limitation of this study is that only the PET acquisition was gated, and one single CT was used for attenuation correction of all PET gates. This approach inherently involves some misregistration between the PET and CT datasets and could potentially introduce artefacts due to a biased attenuation correction [18, 26]. Although the possibility of acquiring respiratory gated or respiratory averaged CT for attenuation correction has been proposed [27], its clinical benefit has not yet been established, and it was decided to perform a single CT in order to avoid the substantial additional radiation for the patient.

The incremental value of dual gating and the associated gain in effective spatial resolution is still undetermined and

Fig. 7 Coronal view of the left ventricle from an ammonia examination. **a** Static view. **b** Dual gated image showing the diastolic expiratory phase. The gated image shows less motional blurring and better resolved myocardial walls
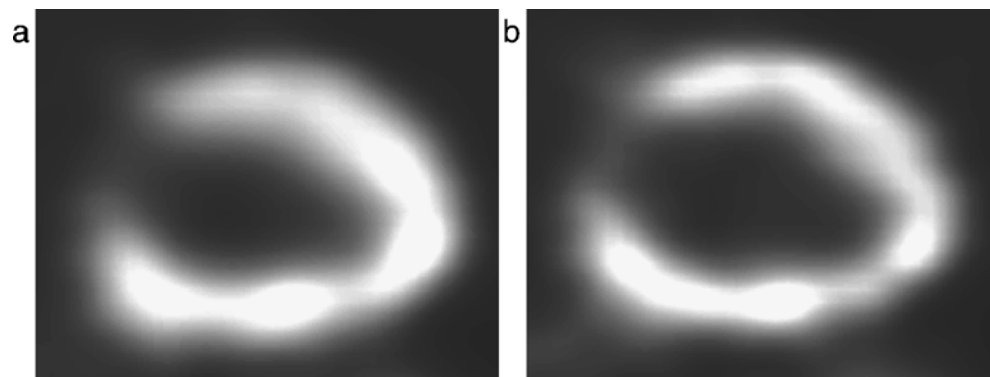
should be further investigated. The effects observed in this study do not seem to justify its use for routine perfusion and metabolic examinations in our clinical setting. However, dual gated acquisitions are likely going to gain importance with the continuous improvement of PET spatial resolution, and it might be speculated that the correction for respiratory motion could be standard in future cardiac applications as it is in cardiac MR. Furthermore, such an approach can be a determinant point for successful hot spot imaging of vulnerable coronary plaques, where the imaged target might be smaller than the combined cardiac–respiratory motion itself.

Conclusion

Dual cardiac–respiratory gated PET was implemented in a clinical PET/CT scanner in a routine setting; thinner and less blurred myocardial walls were observed in the dual gated studies. Flexible sorting of the listmode data allowed for the observation of the respiratory motion of the heart, which was quantified by means of non-rigid image registration and found to average 4.8 mm. Regional motion analysis showed a compression of the heart during breathing, with the inferior wall moving significantly more than the anterior. The incremental value of respiratory motion correction on cardiac PET imaging is still undetermined.

References

1. Schwaiger M, Ziegler S, Nekolla SG. PET/CT: challenge for nuclear cardiology. J Nucl Med 2005;46:1664–78.
2. Kaufmann PA, Camici PG. Myocardial blood flow measurement by PET: technical aspects and clinical applications. J Nucl Med 2005;46:75–88.
3. Matsunari I, Taki J, Nakajima K, Tonami N, Hisada K. Myocardial viability assessment using nuclear medicine [review]. Ann Nucl Med 2003;17:169–79.
4. Pannu HK, Flohr TG, Corl FM, Fishman EK. Current concepts in multi-detector row CT evaluation of the coronary arteries: principles, techniques, and anatomy. Radiographics 2003;23(Suppl):S111–25.
5. Brambilla M, Secco C, Dominietto M, Matheoud R, Sacchetti G, Inglese E. Performance characteristics obtained for a new 3-dimensional lutetium oxyorthosilicate-based whole-body PET/CT scanner with the National Electrical Manufacturers Association NU 2-2001 Standard. J Nucl Med 2005;46:2083–91.
6. Rimoldi O, Schafers KP, Boellaard R, Turkheimer F, Stegger L, Law MP, et al. Quantification of subendocardial and subepicardial blood flow using ^{15}O-labeled water and PET: experimental validation. J Nucl Med 2006;47:163–72.
7. Rudd JHF, Warburton EA, Fryer TD, Jones HA, Clark JC, Antoun N, et al. Imaging atherosclerotic plaque inflammation with [^{18}F]-fluorodeoxyglucose positron emission tomography. Circulation 2002;105:2708–11.
8. Bengel FM, Anton M, Richter T, Simoes MV, Haubner R, Henke J, et al. Noninvasive imaging of transgene expression by use of positron emission tomography in a pig model of myocardial gene transfer. Circulation 2003;108:2127–33.
9. Ter-Pogossian MM, Bergmann SR, Sobel BE. Influence of cardiac and respiratory motion on tomographic reconstructions of the heart: implications for quantitative nuclear cardiology. J Comput Assist Tomogr 1982;6:1148–55.
10. Wang Y, Vidan E, Bergman GW. Cardiac motion of coronary arteries: variability in the rest period and implications for coronary MR angiography. Radiology 1999;213:751–8.
11. Shechter G, Ozturk C, Resar JR, McVeigh ER. Respiratory motion of the heart from free breathing coronary angiograms. IEEE Trans Med Imag 2004;23:1046–56.
12. Boucher L, Rodrigue S, Lecomte R, Bénard F. Respiratory gating for 3-dimensional PET of the thorax: feasibility and initial results. J Nucl Med 2004;45:214–9.
13. Danias PG, Stuber M, Botnar RM, Kissinger KV, Edelman RR, Manning WJ. Relationship between motion of coronary arteries and diaphragm during free breathing: lessons from real-time MR imaging. Am J Roentgenol 1999;172:1061–5.
14. Klein GJ, Reutter BW, Hol MH, Reed JH, Huesman RH. Real-time system for respiratory-cardiac gating in positron tomography. IEEE Trans Nucl Sci 1998;45:2139–43.
15. Yang Y, Rendig S, Siegel S, Newport DF, Cherry SR, Cardiac PET imaging in mice with simultaneous cardiac and respiratory gating. Phys Med Biol 2005;50:2979–89.
16. Livieratos L, Rajappan K, Stegger L, Schafers K, Bailey DL, Camici PG. Respiratory gating of cardiac PET data in list-mode acquisition. Eur J Nucl Med Mol Imaging 2006;33: 584–8.
17. Wang Y, Riederer SJ, Ehman RL. Respiratory motion of the heart: kinematics and implications for the spatial resolution in coronary imaging. Magn Reson Med 1995;33:713–9.
18. Martinez-Möller A, Souvatzoglou M, Navab N, Schwaiger M, Nekolla SG. Artifacts from misaligned CT in cardiac perfusion PET/CT studies: frequency, effects and potential solutions. J Nucl Med 2007;2:188–93.
19. Modersitzki J. Numerical methods for image registration. Oxford; Oxford University Press; 2004.
20. Briggs WL, Henson VE, MacCormick SF. A multigrid tutorial. Philadelphia, PA; Society for Industrial and Applied Mathematics; 2000.
21. Álvarez L, Weickert J, Sánchez J. Reliable estimation of dense optical flow fields with large displacements. Int J Comput Vision 2000;39:41–56.
22. McLeish K, Hill DLG, Atkinson D, Blackall JM, Razavi R. A study of the motion and deformation of the heart due to respiration. IEEE Trans Med Imag 2002;21:1142–50.
23. Livieratos L, Stegger L, Bloomfield PM, Schafers K, Bailey DL, Camici PG. Rigid-body transformation of list-mode projection data for respiratory motion correction in cardiac PET. Phys Med Biol 2005;50:3313–22.
24. Klein GJ, Reutter BW, Huesman RH. Four-dimensional affine registration models for respiratory-gated PET. IEEE Trans Nucl Sci 2001;48:756–60.
25. Manke D, Nehrke K, Rosch P, Bornert P, Dossel O. Study of respiratory motion in coronary MRA. Proc. 9th Annu. Meeting ISMRM, Glasgow, UK, 2001, no. 1852.
26. Osman MM, Cohade C, Nakamoto Y, Wahl RL. Respiratory motion artifacts on PET emission images obtained using CT attenuation correction on PET-CT. Eur J Nucl Med Mol Imaging 2003;30:603–6.
27. Pan T, Mawlawi O, Nehmeh SA, Erdi YE, Luo D, Liu HH, et al. Attenuation correction of PET images with respiration-averaged CT images in PET/CT. J Nucl Med 2005;46:1481–7.